kJ/mol of the calculated global minimum energy conformer (*8*). Whereas the glycosidic torsion angles of the αD-Abe(1 → 3)αD-Man linkage in the bound epitope agree reasonably well with the predicted values (ϕ, ψ of 80°, 91°, versus calculated values of 66°, 106°, where ϕ = O5-C1-O1-C′*x*, and ψ = C1-O1-C′*x*-C′*x*+1), the torsion angle of the αD-Gal(1 → 2)αD-Man linkage adopts a ϕ value that is shifted about 40° (ϕ, ψ of 105°, 83° versus calculated values of 68°, 101°) from the value of 60° to 70° that is generally anticipated from a consideration of the exo-anomeric effect (*21*) and is observed in crystal structures of methyl glycosides and oligosaccharides (*22*). The ϕ angle adopted by the galactose-mannose linkage is essential for an intramolecular scheme of conjugated hydrogen bonds that begin at Gly 98H and connect O-2 of abequose, O-2 of galactose, and O-1 of abequose. Potential energy calculations that include a hydrogen-bonding term indicate that unfavorable stereoelectronic and nonbonded interactions that result from the changed ϕ angle are offset by the intersaccharide hydrogen bonds.

In response to this bacterial antigen, the immune system has used somatic mutation of germ line genes (seven residues in the λ CDRs) to generate a carbohydrate binding site that is notably different from those previously investigated by crystallography. Although polar and planar side chains of the dicarboxylic amino acids have been identified as main features of hydrogen-bonding networks to sugars in carbohydrate binding proteins (*19*), this site is almost exclusively defined by aromatic amino acids. This result confirms inferences about the increased frequency of the use of aromatic amino acids in antibody CDRs (*23*). The abequose and the mannose are hydrogen-bonded to the side chains of His and Trp residues. The presence of three His residues in the CDRs contacting the saccharide probably results in the unusually mild dissociation pH, which corresponds to an approximate His pK_a of 5.6. At present, there is no way to differentiate between the three His residues that contact the epitope, but two of the imidazole rings (His 35H and His 97H) are thought to be neutral in the crystal.

This crystal structure shows that binding sites that use neutral amino acid hydrogen-bonding partners can have relatively high affinity for oligosaccharide epitopes. The conformation seen in the bound state, although fairly well modeled by simple potential energy calculations, is strongly influenced by the requirements for highly complementary surfaces and hydrogen-bonding networks (*19*). Hydroxyl groups that act as hydrogen-bond acceptors must also successfully donate a hydrogen bond to a neighboring acceptor (*24*). Here the functional groups that fulfill this role are a water molecule, other hydroxyl groups, and ring or exocyclic oxygen atoms occurring in acetal linkages. The inferred hydrogen-bonding scheme is also consistent with functional group replacement studies (*25*). The crystal structure described here, in combination with the use of synthetic gene technology to clone and express this Fab (*26*) and its fully active single-chain Fv fragment (*27*), provides the opportunity to engineer carbohydrate binding sites and to explore the importance of the different hydrogen-bond types for the stability of the carbohydrate-protein complexes.

REFERENCES AND NOTES

1. J. B. Robbins, *Immunochemistry* **15**, 839 (1978); J. Thurin, *Curr. Top. Microbiol. Immunol.* **139**, 59 (1988).
2. A. N. Houghton *et al.*, *Proc. Natl. Acad. Sci. U.S.A.* **82**, 1242 (1985).
3. C. P. J. Glaudemans, *Mol. Immunol.* **24**, 371 (1987); R. U. Lemieux, R. Cromer, U. Spohr, *Can. J. Chem.* **66**, 3083 (1988); R. U. Lemieux, *Chem. Soc. Rev.* **18**, 347 (1989).
4. E. M. Nashel *et al.*, *J. Biol. Chem.* **265**, 20699 (1990); E. A. Padlan and E. A. Kabat, *Proc. Natl. Acad. Sci. U.S.A.* **85**, 6885 (1988).
5. D. R. Bundle, *Top. Curr. Chem.* **154**, 1 (1990).
6. O. Lüderitz, A. M. Staub, O. Westphal, *Bacteriol. Rev.* **30**, 192 (1966).
7. F. Kauffmann, *The Bacteriology of Enterobacteriaceae* (Munksgaard, Copenhagen, 1966).
8. K. Bock *et al.*, *Carbohydr. Res.* **130**, 23 (1984).
9. K. Bock *et al.*, *ibid.*, p. 35.
10. B. Sigurskjold, E. Altman, D. R. Bundle, *Eur. J. Biochem.* **197**, 239 (1991).
11. D. R. Rose *et al.*, *J. Mol. Biol.* **215**, 489 (1990).
12. A. T. Brunger, X-plor, A System for Crystallography and NMR, 2.1, manual (Yale University, New Haven, CT, 1990).
13. A. T. Jones, *J. Appl. Crystallogr.* **11**, 614 (1978).
14. D. A. Case and M. Karplus, *J. Mol. Biol.* **132**, 343 (1979).
15. M. L. Connolly, *J. Appl. Crystallogr.* **16**, 548 (1983).
16. J. N. Herron, X.-M. He, M. L. Mason, E. W. Voss, Jr., A. B. Edmundson, *Proteins* **5**, 271 (1989).
17. R. L. Stanfield, T. M. Fieser, R. A. Lerner, I. A. Wilson, *Science* **248**, 712 (1990).
18. A. G. Amit, R. A. Mariuzza, S. E. V. Phillips, R. J. Poljak, *ibid.* **233**, 747 (1986); S. Sheriff *et al.*, *Proc. Natl. Acad. Sci. U.S.A.* **84**, 8075 (1987); E. A. Padlan *et al.*, *ibid.* **86**, 5938 (1989).
19. F. A. Quiocho, *Annu. Rev. Biochem.* **55**, 287 (1986).
20. L. N. Johnson *et al.*, *Curr. Top. Microbiol. Immunol.* **139**, 81 (1988).
21. R. U. Lemieux, S. Koto, D. Voisin, *ACS Symp. Ser.* **87**, 17 (1979).
22. S. Pérez and R. H. Marchessault, *Carbohydr. Res.* **65**, 114 (1978).
23. E. A. Padlan, *Proteins* **7**, 112 (1990).
24. F. A. Quiocho, D. K. Wilson, N. K. Vyas, *Nature* **300**, 404 (1989).
25. D. R. Bundle, unpublished results.
26. N. N. Anand *et al.*, *Gene*, in press.
27. N. N. Anand *et al.*, *J. Biol. Chem.*, in preparation.
28. Abbreviations for the amino acid residues are as follows: A, Ala; C, Cys; D, Asp; E, Glu; F, Phe; G, Gly; H, His; I, Ile; K, Lys; L, Leu; M, Met; N, Asn; P, Pro; Q, Gln; R, Arg; S, Ser; T, Thr; V, Val; W, Trp; and Y, Tyr.
29. National Research Council publication 32764.

4 February 1991; accepted 30 April 1991

Solution Structure of Kistrin, a Potent Platelet Aggregation Inhibitor and GP IIb-IIIa Antagonist

MARC ADLER, ROBERT A. LAZARUS, MARK S. DENNIS, GERHARD WAGNER*

The structure of kistrin, which is a member of a homologous family of glycoprotein IIb-IIIa (GP IIb-IIIa) antagonists and potent protein inhibitors of platelet aggregation, has been determined by two-dimensional nuclear magnetic resonance (NMR) spectroscopy. The 68-residue protein consists of a series of tightly packed loops held together by six disulfide bonds and has almost no regular secondary structure. Kistrin has an Arg-Gly-Asp (RGD) adhesion site recognition sequence important for binding to GP IIb-IIIa that is located at the apex of a long loop across the surface of the protein.

KISTRIN IS A POTENT PROTEIN INhibitor of platelet aggregation that occurs naturally and has recently been isolated from the venom of the Malayan pit viper *Agkistrodon rhodostoma* (*1*). Platelet aggregation is mediated by the interaction of a surface GP IIb-IIIa with plasma fibrinogen (Fg) and leads to the formation of platelet-rich clots, the inhibition of which may have beneficial affects for arterial thrombotic diseases (*2*). GP IIb-IIIa is a member of a family of glycoproteins called integrins, which are a large class of cell surface receptors that play important roles in cell-matrix and cell-cell adhesion (*3, 4*). Extracellular matrix ligands such as Fg, fibronectin, vitronectin, or von Willlebrand factor that bind to GP IIb-IIIa and other integrins all contain the RGD adhesion site recognition sequence thought to be critical

M. Adler and G. Wagner, Department of Biological Chemistry and Molecular Pharmacology, Harvard Medical School, Boston, MA 02115.
R. A. Lazarus and M. S. Dennis, Department of Protein Engineering, Genentech, Inc., South San Francisco, CA 94080.

*To whom correspondence should be addressed.

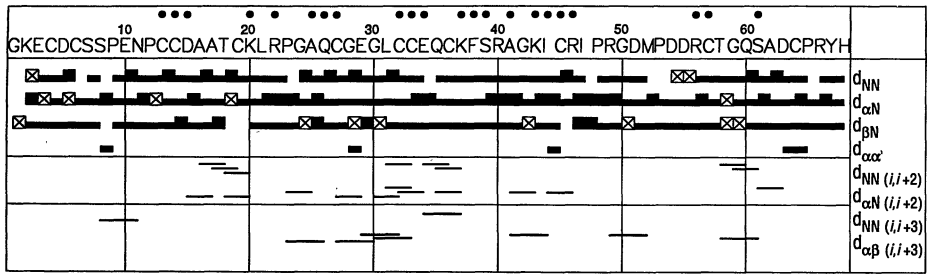

Fig. 1. Summary of sequential and medium-range NOEs. Solid circles above the letter for a residue represent a slowly exchanging amide proton. For the sequential NOEs three symbols are used. A thick bar is for NOEs observed in a NOESY with a mixing time of 60 ms. The thinner line indicates an observable NOE at longer mixing times (200 ms). The symbol ☒ is used for cross peaks that are obscured by overlaps or are too close to the water line; therefore, the existence of these peaks cannot be verified.

for binding (*3, 5, 6*). Kistrin, a member of the family of homologous proteins from viper venoms (*1, 7*), contains 68 amino acids (Fig. 1) and six intramolecular disulfide bonds. It also has an RGD sequence and binds reversibly to GP IIb-IIIa with nanomolar affinity (*1*). Therefore, knowledge of the structure of kistrin, when combined with data from site-directed mutagenesis (*8*), may provide some insight into its binding interactions to GP IIb-IIIa and into the structure of other members of this family.

Backbone proton resonances of all residues have been assigned except the NH_2-terminal Gly, whose assignment cannot be confirmed because of problems with overlapping resonances (*9*). Also, all but 35 nonexchanging side-chain protons have been identified (*10*). To date, 549 interresidue nuclear Overhauser effect (NOE) connectivities have been assigned from two-dimensional NOE (NOESY) spectra with 200-ms mixing times (*11*). These observed NOEs were categorized in three classes. All cross peaks that were observed in 200-ms NOESY spectra were associated with upper distance limits of 5 Å. Cross peaks observed in NOESY spectra with mixing times of 80 ms or less were classified as weak and strong with upper distance limits of 4.5 and 3.5 Å, respectively.

Of the 549 NOEs, 255 connected sequential residues. Only 91 of these sequential NOEs represent "useful" information, that is, the upper distance limit determined by the NOE intensity is smaller than the maximum distance allowed by the covalent geometry. The data set contains a total of 78 medium-range NOEs ($3 \leq i - j \leq 5$) and 216 long-range NOEs ($6 \leq i - j$); 147 NOEs connect residues that were separated by more than ten residues. There are on average 5.7 "useful" NOE constraints per residue.

In addition, we have included information about 25 ϕ and 25 χ^1 angles in the structure calculation. Constraints on the angle ϕ were derived from NH to CαH coupling constants in a way similar to that described by Kline *et al.* (*12*). Thus, only NH to CαH coupling constants that were less than 5.5 Hz or greater than 8.0 Hz were used. The values of χ^1 and the stereospecific assignments of the attached CβHs were determined with the procedure as described (*13*). We enforced angle constraints by specifying ranges for all 1-4 distances surrounding the bond. Model calculations showed that this procedure gave a smooth potential with no local minima and zero penalty when the angle was within the specified range. The technique was 80 to 90% successful at maintaining the appropriate dihedral angles.

There are six prolines in kistrin. Intense $C\alpha H_{(i)}$ to $C\delta H_{(i+1)}$ cross peaks firmly establish that all six are trans prolines (*14*). Several of the prolines appear in the second position of β turns.

Disulfide pairings were determined by searching for CβH to CβH and CαH to CβH NOEs between different cysteines. For five of the six cysteine pairs at least one intercysteine NOE could be found. In cases where one cysteine showed NOEs to more than one other cysteine, there was numerical preference for one pairing over the other. However, model calculations (*15*) demonstrated that there are conformations of the disulfide bonds with no interresidue proton distances of 5 Å or less. Therefore, initial structure calculations were performed without any explicit disulfide bonds. Visual inspection of the structures either confirmed the initial pairing or, in about 10% of the calculations, did not clearly indicate a satisfactory pairing for cysteines 4, 6, 14, and 19. When this visual information was combined with chemical evidence for disulfide bonds obtained by Carter *et al.* (*16*), there was only one possible pairing for all six disulfide bonds. The results agree exactly with our initial assignments, and the explicit disulfide bonds (between 4 and 19, 6 and 14, 13 and 36, 27 and 33, 32 and 57, and 45 and 64) were included in the subsequent calculations.

The diagonal map of NOEs (Fig. 2) shows little evidence for any regular secondary structure in kistrin. Indeed, the only section of the protein that is completely consistent with regular structure is a partial antiparallel β sheet structure formed by res-

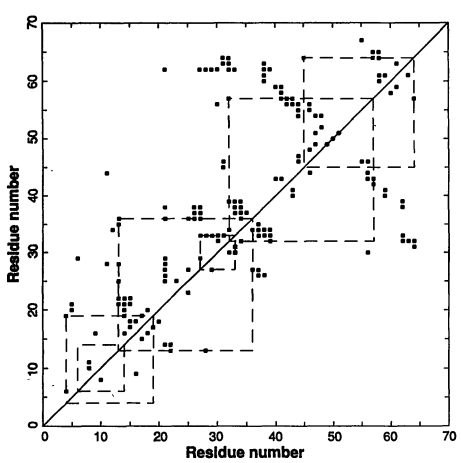

Fig. 2. Diagonal plot of interresidue NOEs. Points above the diagonal represent an NOE between any two nonsequential residues. Below the diagonal, only backbone NOEs are plotted. The dotted lines represent the six disulfide bonds in kistrin. The three small circles on the diagonal mark the RGD sequence.

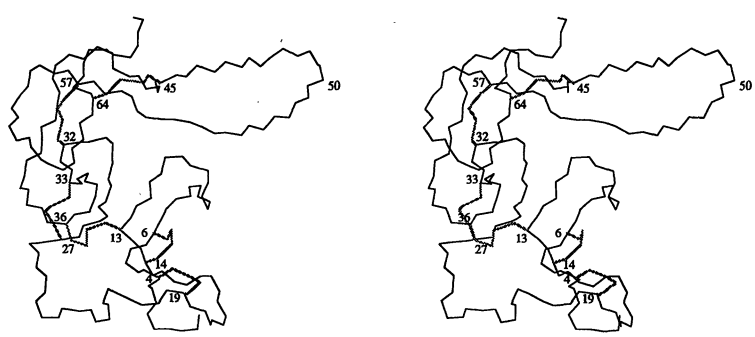

Fig. 3. Stereoview of the kistrin structure containing the lowest violation of the constraints with the backbone atoms displayed. The side-chain atoms of the 12 cysteines have been drawn in gray and the Cαs have been labeled. The Cα of G50 has also been labeled.

idues 34 and 37. A large number of interstrand NOEs indicate that there may be an antiparallel β sheet and turn extending from residues 41 to 59. The RGD adhesion site, residues 49 to 51, is located at the apex of the turn. However, the chain stretching from residues 41 to 49 has several i to $i + 2$ and i to $i + 3$ NOEs. These results cannot be reconciled with a standard β sheet. Therefore, only two explicit hydrogen bonds, between residues 34 and 37, were added to the constraint file. The lack of regular structure is somewhat surprising because kistrin has 23 slowly exchanging amide protons (Fig. 1). Reasonable hydrogen bond acceptors can be identified at present for 12 of the slowly exchanging NHs but have not been included in the calculation.

The protein consists of a series of densely packed bends (Fig. 3) (*17*). On the basis of evidence from the sequence, the structure calculations, and the position of slowly exchanging amides, six potential β turns have been identified in the first 37 residues. However, no explicit constraints have been included for these, and some conformational heterogeneity is apparent in the β turns (Figs. 3 and 4). The conformation of the first turn at S8-P9-E10-N11 is the least firmly established, but the presence of the trans proline in the second position is a strong indication of a β turn. The next three β turns are located at N11-P12-C13-C14, A16-A17-T18-C19, and R22-P23-G24-A25. The loop that contains the β turn at residues 16 to 19 is pointing downward in Fig. 3. The fifth β turn, G30-L31-C32-C33, is unusual in that it is buried within the protein. A potential hydrogen bond donor, γOH of S39, and acceptor, CO of residue A62, have been identified for both the NH and CO of the peptide group located at the apex of the bend. The sixth β turn, E34-Q35-C36-K37, forms a bridge between upper and lower parts of the protein and is facing out of the page in Fig. 3. Slowly exchanging amides located at residues C14, A25, C33, and K37 are consistent with a hydrogen bond between the carboxyl and amide of the first and fourth residues of these β turns (*18*), thus confirming the existence of four of the six turns. The structure calculations have yet to consistently indicate β turns in other parts of the protein.

The RGD adhesion site, residues 49 to 51, lies at the end of a long arm consisting of two antiparallel strands, residues 41 to 47 and 52 to 59. The arm curls over the β turn at residues 30 to 33 and then extends out over N11. There are seven medium-range NOEs for residues 47 to 53, but no long-range NOEs. The calculations have consistently determined this loop to be in a fairly extended conformation where the loop residues have little contact with the rest of the molecule. However, there is no direct evidence for this conformation, and its orientation relative to the protein core may be less well defined than it appears from Fig. 4. The adhesion site itself is located between two bends created by trans prolines 48 and 53, and the local conformation is, to some extent, restricted by the medium-range NOEs and constraints on the angle φ for residues 51 and 52. The average Cα to Cα distance for R49 to D51 is 6.2. ± 0.6 Å, compared to 7.0 Å for a β sheet, which is consistent with a fairly extended conformation. The structure of kistrin culminates in a broad loop formed from residues 58 to 64, which partially covers the β turn at residues 30 to 33. The positions of residues 4 to 46 and 56 to 64 are the most accurately determined positions in the protein, showing a backbone root-mean-square (rms) deviation of 1.0 Å when compared to the averaged coordinates. The NH_2- and COOH-termini and the adhesion site itself are fairly disordered (Fig. 4). The rms deviation between all heavy atoms is 1.5 Å.

The global fold of kistrin is probably maintained by the six disulfide bonds. At least one-half of the cysteines are located inside β turns. This suggests a possible folding mechanism. The initial stages of folding would consist of formation of the β turns. Contact between turns would provide cooperative stabilization, followed by oxidation of the cysteines to lock the protein into its final conformation.

Kistrin, as well as several other protein GP IIb-IIIa antagonists from snake venoms or leeches, inhibits platelet aggregation induced by adenosine diphosphate about 100 to 1000 times more potently than do short, linear peptides containing RGD (*1, 7, 19, 20*). The enhanced binding affinity to GP IIb-IIIa observed in these proteins is likely due to favorable conformational restraints of the RGD sequence, not the presence of major secondary binding determinants. This conclusion is now supported by (i) the presence of the RGD adhesion site at the apex of the putative binding loop, (ii) the lack of homology outside of the RGD region between the equipotent leech proteins decorsin or ornatin (*19*) and the snake venom antagonists, (iii) the fact that replacement of the RGD sequence in echistatin (*20*) or kistrin (*8*) with other amino acids leads to significantly less potent proteins, and (iv) data from relatively small constrained cyclic peptides containing RGD that have potencies comparable to those of the natural protein GP IIb-IIIa antagonists (*21*).

Recently, kistrin has been shown to increase both the rate and extent of the thrombolysis and prevent reocclusion when used in conjunction with a recombinant tissue-type plasminogen activator in a canine model of coronary artery thrombosis (*22*). Therefore, further refinement of the structure of the binding region may aid in the design of new GP IIb-IIIa antagonists for the treatment of arterial thrombotic disease.

Fig. 4. Stereoview of the superimposed six computed kistrin structures. For the alignment of the structures only the residues 4 to 46 and 56 to 64 were used. The average rms deviation in this part of the molecule is 1.0 Å for the backbone atoms.

REFERENCES AND NOTES

1. M. S. Dennis *et al.*, *Proc. Natl. Acad. Sci. U.S.A.* **87**, 2471 (1990).
2. B. Stein *et al.*, *J. Am. Coll. Cardiol.* **14**, 813 (1989); J. Hawiger, *Atheroscler. Rev.* **21**, 165 (1990); R. C. Becker and J. M. Gore, *Circulation* **83**, 1115 (1991).
3. D. R. Phillips, I. F. Charo, L. V. Parise, L. A. Fitzgerald, *Blood* **71**, 831 (1988); E. F. Plow and M. H. Ginsburg, in *Progress in Hemostasis and Thrombosis*, B. S. Coller, Ed. (Saunders, Philadelphia, 1989), vol. 9, pp. 117–1156.
4. R. O. Hynes, *Cell* **48**, 549 (1987); S. M. Albelda and C. A. Buck, *FASEB J.* **4**, 2868 (1990).
5. E. Ruoslahti and M. D. Pierschbacher, *Science* **238**, 491 (1987).
6. Abbreviations for the acid residues are as follows: A, Ala; C, Cys; D, Asp; E, Glu; F, Phe; G, Gly; H, His; I, Ile; K, Lys; L, Leu; M, Met; N, Asn; P, Pro; Q, Gln; R, Arg; S, Ser; T, Thr; V, Val; W, Trp; and Y, Tyr.

7. R. J. Gould *et al.*, *Proc. Soc. Exp. Biol. Med.* **195**, 168 (1990).
8. M. S. Dennis, P. Carter, R. A. Lazarus, in preparation.
9. NMR measurements were performed on a GN-500 spectrometer. The majority of the measurements were made with 5 mM kistrin at pH 2.2 and 20°C. Preliminary analysis of the two-dimensional NMR spectra indicates that there is no significant conformational shift between pH 7 and pH 2.2 at 20°C (M. Adler and G. Wagner, unpublished results); the structure published here should be comparable to that at neutral pH.
10. M. Adler, R. A. Lazarus, M. S. Dennis, G. Wagner, in preparation.
11. NOEs are effects arising from dipole-dipole interactions between protons that are close in space. Such interactions usually give rise to cross peaks in NOESY spectra if the protons are separated by less than ~5 Å. The symbols *i*, *j*, and *i* + *a* are used as indices for the two residues connected by an NOE. NOEs with values of *i* to *i* + 2 indicate turns or helices.
12. A. D. Kline, W. Braun, K. Wüthrich, *J. Mol. Biol.* **204**, 675 (1988).
13. G. Wagner *et al.*, *ibid.* **196**, 611 (1987).
14. K. Wüthrich, M. Billeter, W. Braun, *ibid.* **180**, 715, (1984); G. T. Montelione, P. Hughes, J. Clardy, H. A. Scheraga, *J. Am. Chem. Soc.* **108**, 6765 (1986).
15. M. Adler and G. Wagner, unpublished results.
16. P. Carter *et al.*, unpublished results.
17. We performed the calculations as follows using the program Dspace (Hare Research, Inc., Woodinville, WA). The structures were first embedded and then minimized with a conjugate gradient against a constraint file based on the NOEs alone. The 1-4 constraints that enforce the 40 angle constraints were then introduced, and the penalties that regulate the integrity of the covalent structure (1-2, 1-3, and 1-4 distance bounds) were increased tenfold over the NOE penalty functions. After some further minimization, an exhaustive round of simulated annealing was performed, followed by minimization. At this point, the structures with no NOE violations in excess of 0.7 Å were selected and subjected to 40 rapid rounds of simulated annealing followed by minimization. Roughly 1 out of 20 structures had no NOE violations over 0.5 Å. (Two-thirds of the structures had no violations greater than 1 Å). There were on average two violations of the covalent structure over 0.1 Å, and some structures had no violations this large. A large number of the residual violations centered around C45. This residue has a disulfide bond to C64 and appears in roughly the third position of a tight bend. The disulfide bond itself passes under (and sometimes over) residues R56-C57 (Fig. 3). This geometry apparently stretches the disulfide bond and causes distortion in the covalent geometry of the flanking residues. This problem has yet to be resolved and it may in part stem from spin diffusion effects causing overinterpretation of the NOEs to the methyl groups of I44.
18. J. Richardson, *Adv. Protein Chem.* **34**, 167 (1981).
19. J. L. Seymour, W. J. Henzel, B. Nevins, J. T. Stults, R. A. Lazarus, *J. Biol. Chem.* **265**, 10143 (1990); P. Mazur, W. J. Henzel, J. L. Seymour, R. A. Lazarus, in preparation.
20. V. M. Garsky *et al.*, *Proc. Natl. Acad. Sci. U.S.A.* **86**, 4022 (1989).
21. A. Nichols *et al.*, *Eur. J. Pharmacol.* **183**, 2019 (1990); P. L. Barker, J. P. Burnier, T. Gadek, E. D. Thorsett, Pat. Coop. Treaty Intl. Appl. WO 91, 01331 (1991).
22. T. Yasuda *et al.*, *Circulation* **83**, 1038 (1991).
23. We thank Dow Chemical Company for a fellowship to M. A. V. Thanabal for assistance in using the spectrometer, Hare Research for their generous donation of the programs FTNMR and Dspace, and T. Kossiakoff and R. McDowell for helpful discussions. Partial support from NIH grant GM38608 is also acknowledged. NMR spectrometer acquired with a grant from NSF (BBS-8615223). The coordinates of the structure have been submitted to the Brookhaven Protein Data Bank.

19 February 1991; accepted 8 May 1991

Identification of a Mutation in Porcine Ryanodine Receptor Associated with Malignant Hyperthermia

JUNICHI FUJII,* KINYA OTSU, FRANCESCO ZORZATO,† STELLA DE LEON, VIJAY K. KHANNA, JANICE E. WEILER, PETER J. O'BRIEN, DAVID H. MACLENNAN‡

Malignant hyperthermia (MH) causes neurological, liver, and kidney damage and death in humans and major economic losses in the swine industry. A single point mutation in the porcine gene for the skeletal muscle ryanodine receptor (*ryr1*) was found to be correlated with MH in five major breeds of lean, heavily muscled swine. Haplotyping suggests that the mutation in all five breeds has a common origin. Assuming that this is the causal mutation for MH, the development of a noninvasive diagnostic test will provide the basis for elimination of the MH gene or its controlled inclusion in swine breeding programs

MH IS AN INHERITED MYOPATHY in which skeletal muscle contracture with attendant hypermetabolism and elevation in body temperature are triggered by inhalational anesthetics and skeletal muscle relaxants (*1, 2*). The syndrome occurs in one out of 15,000 anesthetized children and one out of 50,000 anesthetized adult humans; can cause neurological, liver, or kidney damage; and is frequently fatal. In swine homozygous for the defect, MH can also be triggered by stress; thus the disease is referred to as the porcine stress syndrome. Major economic losses in the swine industry result from the development of pale, soft, exudative pork that arises from postmortem manifestation of the disease in MH susceptible (MHS) animals (*1*).

The defect in MH appears to be hypersensitive gating of the Ca^{2+}-release channel (ryanodine receptor) of the skeletal muscle sarcoplasmic reticulum (*3*); channel opening is facilitated, and closing is inhibited (*3–6*). Alterations in the Ca^{2+} dependence of ryanodine binding (*7*) and tryptic digestion patterns (*8*) for the ryanodine receptor from MHS swine have been observed. Molecular genetic studies also associate an altered ryanodine receptor with MH. The skeletal muscle ryanodine receptor (*ryr1*) gene, which is expressed only in fast- and slow-twitch skeletal muscle (*9–11*), has been localized to human chromosome 19q13.1 (*12*) and linked to mutations causing MH in humans (*13*). The porcine MH (*hal*) locus (*14*) and *ryr1* (*15*) have been localized to pig chromosome 6p11-q21 in a region that is related to human chromosome 19q13.1, suggesting linkage between porcine MH and *ryr1*. We have identified a single point mutation in *ryr1* that is correlated with, and likely to be causative of, MH in five lean, heavily muscled breeds of swine.

In a sequence comparison of full-length ryanodine receptor cDNAs from both an MHS Pietrain pig and an MH normal (MHN) Yorkshire pig (*16*), we found no evidence for a deletion or an internal stop codon. Instead we found 18 single nucleotide polymorphisms between the two animals (Table 1). One of the polymorphisms, (replacement of C at nucleotide 1843 from the MHN animal with a T in the cDNA from the MHS animal) (Table 1 and Fig. 1) led to an alteration in amino acid sequence from an arginine at position 615 in the MHN animal to a cysteine in the MHS animal.

In order to provide evidence that the single amino acid alteration is causative of MH, we carried out analysis of the association of the substitution of T for C at nucleotide 1843 with the MH susceptibility status of 182 pigs in six breeds (*17*). We performed blood or muscle biopsies for blind DNA-based analysis (*18*). Genomic DNA was isolated from these biopsies and a 74-bp sequence between nucleotides 1811 and 1884 (Fig. 1) was amplified by the polymerase chain reaction (PCR). Two oligonucleotides (*18*) were used as differential hybridization probes to detect the presence of the C and T alleles in the various breeds (Fig. 2A). Because the mutation deletes a Hin P1 site and creates a Hgi AI site (Fig. 1), we also used loss of the Hin P1 site in the PCR product as an analytical test (Fig. 2B).

Study of the correlation between phenotypic and genotypic diagnosis is complicated by the lack of a well-defined phenotypic test for the N/n genotype (heterozygous MH) and by the fact that a low percentage of

J. Fujii, K. Otsu, F. Zorzato, S. de Leon, V. K. Khanna, D. H. MacLennan, Banting and Best Department of Medical Research, University of Toronto, C. H. Best Institute, Toronto, Ontario, M5G 1L6, Canada.
J. E. Weiler and P. J. O'Brien, Department of Pathology, Ontario Veterinary College, University of Guelph, Guelph, Ontario, N1G 2W1, Canada.

*Present address: Department of Biochemistry, Osaka University Medical School, Osaka, Japan.
†Present address: Istituto di Patologia Generale, Universita di Ferrara, Ferrara, Italy.
‡To whom correspondence should be addressed.